

Stress-induced growth of aluminum nanowires with a range of cross-sections

Fan Ye, Michael J. Burns, and Michael J. Naughton*

Department of Physics, Boston College, 140 Commonwealth Avenue, Chestnut Hill, MA 02467, USA

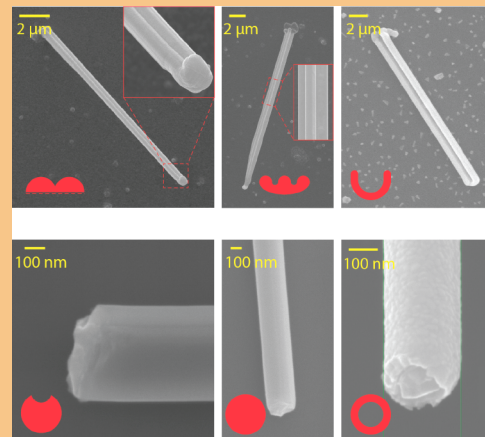
Received 11 August 2014, revised 3 November 2014, accepted 24 November 2014

Published online 00 Month 2014

Keywords aluminum nanowire, nanotube, stress induced growth, surface plasmon polaritons, versatile cross-sections

* Corresponding author: e-mail naughton@bc.edu, Phone: +1 617 552 3575, Fax: +1 617 552 8478

The use of aluminum (Al) as a plasmonic building block has drawn increasing attention of late, due to its natural abundance, and extended tunability into the ultraviolet range. However, a controllable way to grow Al nanowires (NWs) in a bottom-up manner has not been reported. Here a facile, stress-induced growth process for Al nanowires, influenced by the concentration of applied hydrofluoric acid, is reported. Physical characterizations show the nanowires to be polycrystalline fcc Al with ultrasmooth surfaces, with many possible cross-section geometries, making them potential candidates for Al plasmonic investigations and applications. Dark-field optical analysis of a crescent-shaped Al NW demonstrates its plasmonic nature. These results may stimulate new interest in the fabrication of unconventional, nearly one dimensional Al nanostructures.



© 2014 WILEY–VCH Verlag GmbH & Co. KGaA, Weinheim

1 Introduction The use of aluminum (Al) metal as a plasmonic building block has recently drawn increased attention [1–3]. Its natural abundance and extended tunability into the ultraviolet range make Al a promising material for future plasmonic applications [1–3]. To date, Al nanostructures (e.g., 2D nanopatterns and 1D nanowires (NWs), and nanotubes (NTs)) are mainly fabricated by top-down lithographic methods, including electron beam lithography (EBL), nanosphere lithography (NSL), and anodized aluminum oxide (AAO) template lithography [1–6]. For bottom-up, self-assembled growth, wet chemical methods are restricted to the fabrication of noble metal (e.g., Au, Ag, Pt) nanostructures [7–9], though there have been reports of stress-induced [10–12], electromigration-induced [13, 14] and vapor-phase growth in glancing angle deposition [15, 16] of Al microwires and nanowires. The advantages of bottom-up

growth of Al nanostructures are ultra-smoothness and the possibility in formation of 3D structures. Existing bottom-up techniques for Al nanostructures are still in the early development stage, requiring improvements in achieving higher yields, controlling growth conditions and reaching smaller dimensions [10–16].

Here, we report the low temperature (250 °C) stress-induced growth of Al nanostructures on Al-coated glass (SiO₂) wafers controlled by the concentration of applied hydrofluoric (HF) acid. The fabricated Al nanostructures (hereafter referred to collectively as Al NWs) can have ultra-high aspect ratios, ultra-smooth surfaces, and cross-sections with versatile shapes, including ‘kissing circles’, trenches, double wells, crescents, solid cylinders, and tubes. These various self-formed shapes can potentially be exploited for different plasmonic-based applications. For example, metal

cylinders with kissing-circle and crescent cross-sections have been predicted to be useful for broadband plasmonic light harvesting [17, 18]; trenched and double-well cross-section metallic cylinders have been used for gap-mode surface plasmon waveguiding [19, 20]; and metal nanowires and nanotubes can be converted to nano-sized coaxial waveguides by subsequent dielectric-metal coatings for broadband subwavelength waveguiding [21, 22]. We show here that by varying the preparation temperature and the concentration of the HF solution, one can manipulate the growth rate and the yield density of these types of Al NWs. While an effective way to control the shapes of the grown Al NWs remains under development, the method introduced here of stress-induced growth of Al NWs tuned by HF solution suggests the convenient, controllable fabrication of 1D Al nanostructures with unconventional cross-sections.

2 Experimental

2.1 Al NW fabrication The fabrication process of our stress-induced Al NW growth is sketched schematically in Fig. 1. A glass substrate (Fisher 12–550D microscope slide) is cleaned by ultrasonication in acetone, then isopropanol alcohol, and finally water, each for 15 min. An Al layer is then sputtered onto the cleaned glass substrate. The sputtering is done with an Al target in an argon gas plasma at 0.4 Pa, under a DC power of 250 W, with a measured deposition rate of 4 nm/min. The ideal thickness of the Al layer is above ~ 100 nm, because a thinner layer results in Al island formation, while thicker layers result in lower Al NW yield. The Al-coated glass substrate is then baked in air at 250 °C on a hotplate. After the glass substrate has reached the hotplate temperature (within about 2 min), an HF:H₂O solution at room temperature is applied to the substrate by a plastic pipette. Droplets of HF solution evaporate immediately upon contact with the hot Al-coated glass substrate, yielding visible residue areas. The Al-coated glass is kept at 250 °C for another 30 min.

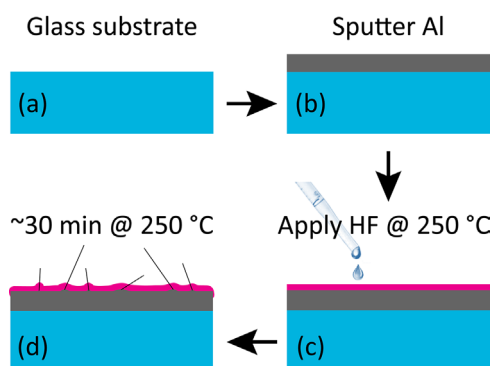


Figure 1 Fabrication of Al nanowires. (a) Cleaned glass substrate. (b) Thin layer of Al (~ 100 nm) sputtered onto the glass substrate. (c) Bake at 250 °C in air, then apply HF solution while heated. Red layer indicates an ~ 5 nm thick native oxide (Al_2O_3) layer. (d) Al NWs sprout up at the local defect sites in regions on the Al film during bake.

When the concentration of the applied HF solution is within an appropriate range, Al NWs grow in the residue areas formed by dried HF droplets. Areas outside of the HF droplet areas only form Al nano- or micro-dots, or hillocks [23, 24].

3 Results and discussion Figure 2 shows SEM micrographs of fabricated Al NWs. Figure 2(a) shows a sideview of the as-grown NWs on the glass substrate. Fig. 2 (b) and (c) show two long Al NWs laying on a Si substrate, with the NW in Fig. 2(b) reaching 100 μm in length, and the one in Fig. 2(c), 40 μm . Fig. 2(d)–(i) show Al NWs with various cross-sections, as sketched in red. The transfer of as-grown Al NWs from the glass substrate to a polished Si substrate is done by pressing the former onto the latter. In this process, some NWs are mechanically broken and/or transfer onto the Si substrate. To directly obtain the shape of cross-sections of the Al NWs, transferred Al NWs are coated (via sputtering) with ~ 250 nm of Ag, then milled by a gallium beam in a focused ion beam (FIB) system. 60° tilted view SEM images of some FIB cross-sections are shown in Fig. 2(j)–(m), reviewing crescent shapes with various radii, and a solid cylinder shape. From the SEM micrographs of the stress-induced Al NWs, we can see that they have diameters ranging from 100 nm to 1 μm , and lengths from 10 μm to 200 μm .

To confirm the composition of the Al NWs, we transferred them onto a Cu grid to carry out TEM observations. Figure 3 shows TEM data for one Al NW with a hollow-circle cross-section (an Al nanotube). Figure 3(a) and (b) show two low magnification images of the same Al NT focused ion beam. The darker edges and brighter center of the Al NT, Fig. 3(b), reveal the tubular structure. Figure 3(c) shows a high magnification image of this Al NT at its boundary, showing a measured atomic distance $d = 0.227 \pm 0.005$ nm. For an fcc Al crystal with lattice constant $a = 0.405$ nm, the atomic distance on the face with Miller index (001) is $d_{001} = 0.234$ nm, matching well with our measured distance. The diffraction TEM image shown in Fig. 3(d) reveals the polycrystalline nature of the Al NT. We thus conclude that the as-prepared Al NT is polycrystalline fcc Al. Energy dispersive spectroscopy data (not shown) on an Al NW also show a slight oxidation of the Al in air.

We performed standard four-probe resistivity measurements (using a Kleindiek nanomanipulator inside the SEM) on one of the Al NTs, as shown in Fig. 4. Figure 4(a) shows a top view SEM image of the four-probe measurement layout. Current was swept between the outer two probes/contacts, and voltage was measured between the inner two, with the resulting I – V curve shown in Fig. 4(b). The geometry of the measured Al NT is estimated to be: length between two inner probes $L \approx 5$ μm , radius of Al NT $r \approx 500$ nm, and thickness of NT wall $t \approx 50$ nm. A least squares fit to the data yields a resistance of $R = 2.9$ Ω , also revealed to be Ohmic by the shown derivative dV/dI . Combined with the geometrical parameters in Fig. 4(b), we obtain an estimated resistivity of $\rho = RS/L \approx 2\pi r t R/L \approx 9.3 \times 10^{-8}$ Ωm . This is comparable to, though somewhat larger than, the bulk

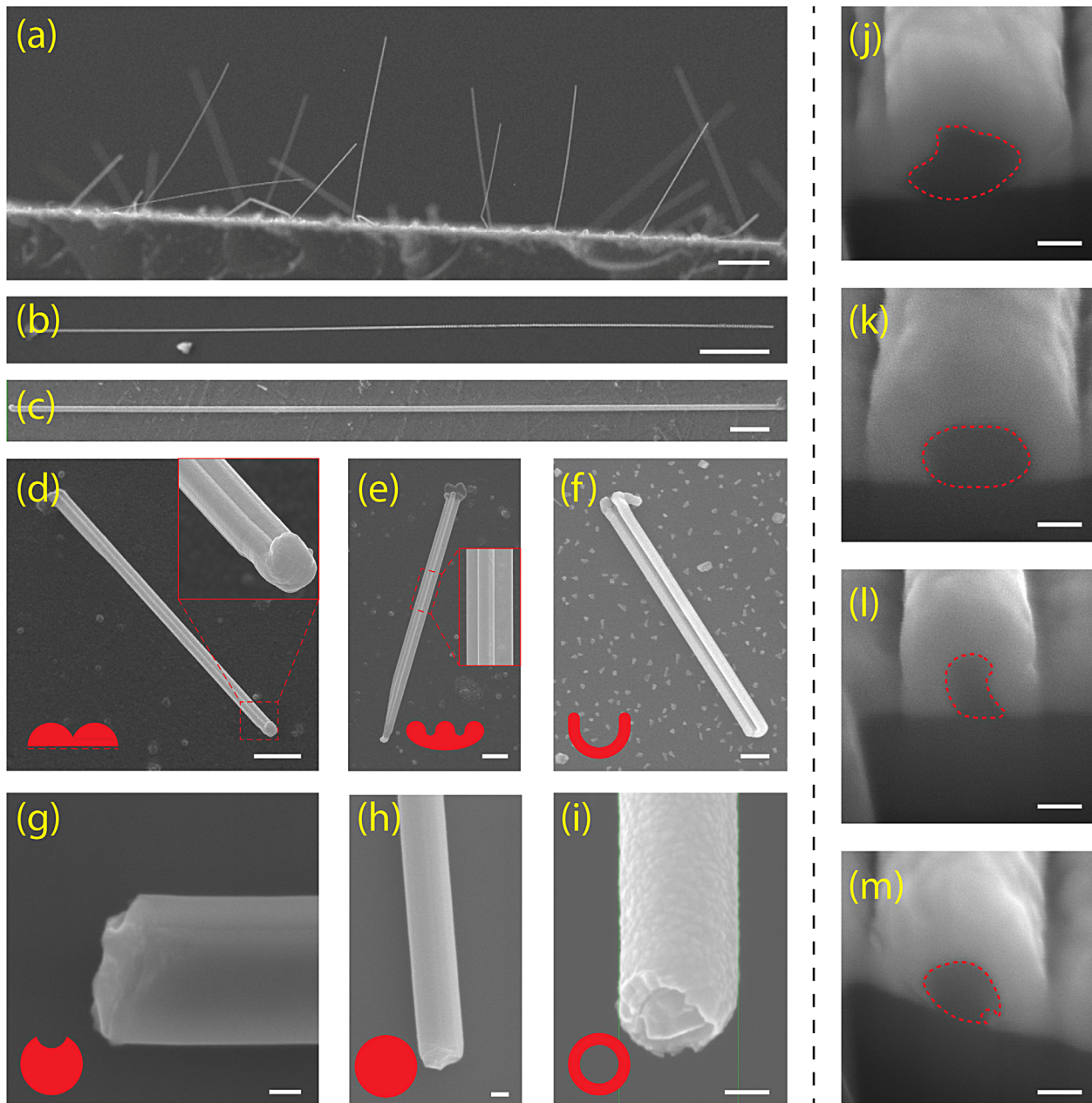


Figure 2 SEMs of Al nanowires with various cross-sections. (a) Side view of Al NWs grown on a glass substrate. (b) 107 μm long NW. (c) 40 μm long NW. (d)–(i) Al NWs with various cross-sections, as sketched in red for each. (j)–(m) SEM images of 60° tilted view of FIB cross-section of Ag coated Al NWs on Si substrate. Red dashed lines indicate cross-section of Al NWs. The bright layer covering the Al NWs is Ag. The dark layer beneath the Al NWs is Si. Scale bars: (a) 20 μm ; (b) 10 μm ; (c)–(f) 2 μm ; (g)–(m) 100 nm.

resistivity of Al, $2.8 \times 10^{-8} \Omega\text{m}$. This resistivity measurement thus confirms the highly conducting (i.e., metallic) nature of the grown Al NWs.

To investigate the role of the HF solution in the growth process, we carried out a control experiment of Al NW growth when applying HF solution with various concentrations in H_2O . Shown in Fig. 5 are dark-field optical images of Al NWs grown on a substrate while tuning the HF concentration. We see that when there is no HF, no Al NWs

grow, with only Al islands formed, as shown in Fig. 5(a). When the HF concentration is high (i.e., HF:H₂O = 1:50), it etches through the Al film and reacts with the bottom SiO₂ layer, leading to no Al NW formation, as shown in Fig. 5(d). Only a restricted range of HF concentration yields Al NWs, as shown in Fig. 5(b) and (c). Note that while Fig. 5(b) and (c) show the center of the HF droplet circles, Fig. 5(d) shows the edge of a HF droplet circle, with the lower left being the inside of the circle (higher HF concentration) and the upper

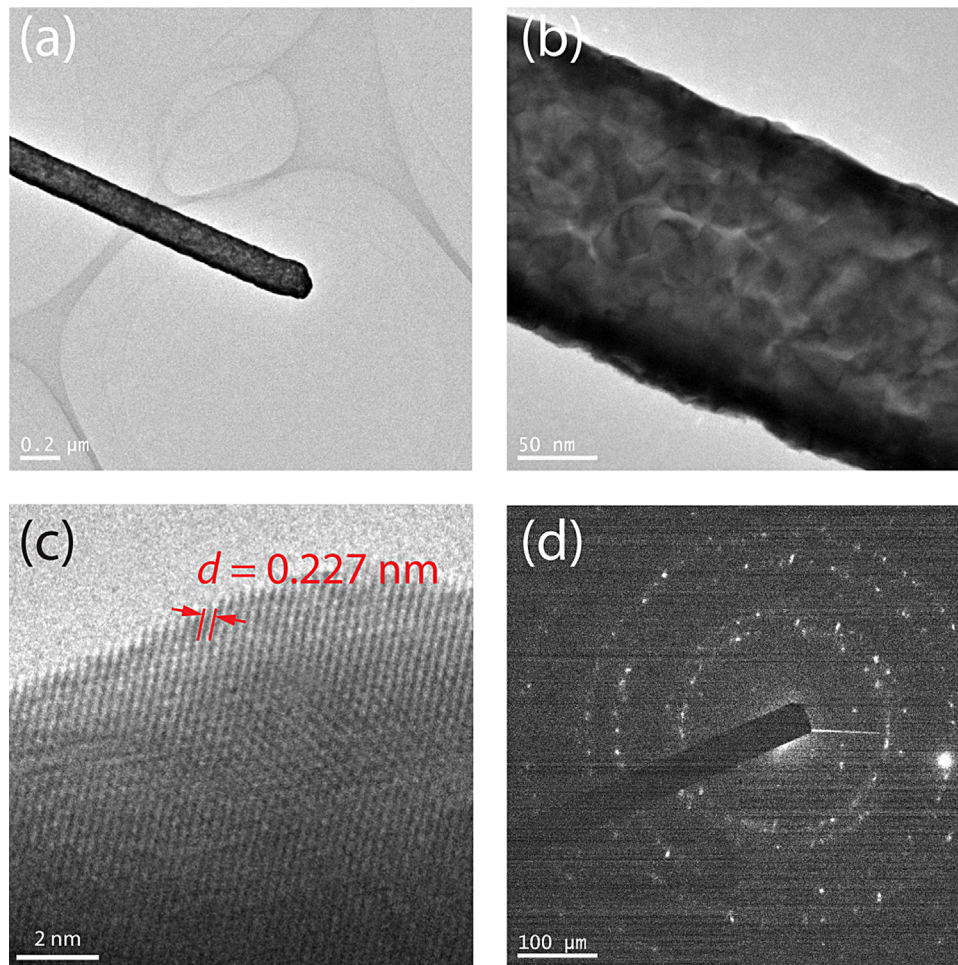


Figure 3 TEM images of an Al nanotube. (a), (b) Low magnification. (c) High magnification, with measured lattice constant indicated. (d) TEM diffraction image of the Al nanotube, showing polycrystalline nature. Scale bars: (a) 0.2 μm ; (b) 50 nm; (c) 2 nm; (d) 100 μm .

right being the outside of it, showing the effect of a concentration gradient. We see that at the lower HF concentration area, there is still Al NW grown (though scarce), as pointed out by a red arrow in Fig. 5(d). The orientations of the as-grown Al NWs appear random, as shown in Fig. 5(b) and (c). The end of a NW that touches the substrate is well focused, while the end pointing up is defocused, resulting in a blurred image. This effect is seen for multiple Al NWs in Fig. 5(b) and (c).

The role of HF solution is inferred to be the following: after baking in ambient conditions at 250 $^{\circ}\text{C}$, a thin native oxide (Al_2O_3) layer is formed on the top surface of the Al film. Thus, the Al film is now sandwiched by the top Al_2O_3 layer and the bottom SiO_2 layer. Due to the high expansion coefficient of Al ($27 \times 10^{-6} \text{K}^{-1}$ at 250 $^{\circ}\text{C}$) [25] relative to that of Al_2O_3 ($7.7 \times 10^{-6} \text{K}^{-1}$ at 250 $^{\circ}\text{C}$) [26] and SiO_2 ($5.3 \times 10^{-6} \text{K}^{-1}$ at 250 $^{\circ}\text{C}$) [27], stress develops within the middle Al layer. As the bottom surface is protected by solid bulk SiO_2 , weak points on the Al_2O_3 surface act as release points for the stress field in the Al film, to which Al metal migrates and extrudes out [12]. HF does not react with

Al_2O_3 , but will potentially react with metallic or organic impurities on the Al_2O_3 surface, opening up weak points on the Al_2O_3 surface for the highly stressed Al underneath. Al atoms then extrude through these weak points via stress-induced migration [12]. Al NWs subsequently form as Al extrudes through nanosized access ports, with cross-sections that follow the shape of the port. Impurities on the Al_2O_3 surface are inferred to come from residual impurities on the glass substrate, perhaps due to inhomogeneous coverage of the thin Al film. Control experiments were done to explore how the cleaning conditions of the glass substrate affect the growth of Al NWs. For glass substrates cleaned under 0.4 Pa argon plasma at 10 mW power for 2 min, no Al NW growth was observed. During the plasma cleaning procedure, organic and/or small metallic impurities on the glass substrate are removed. The absence of Al NWs growth on the plasma-cleaned glass substrate supports our argument that impurities come from the glass substrate.

To demonstrate the plasmonic nature of the extruded Al NWs, we characterized one with a crescent-shaped cross-section via dark field optical microscopy under linearly

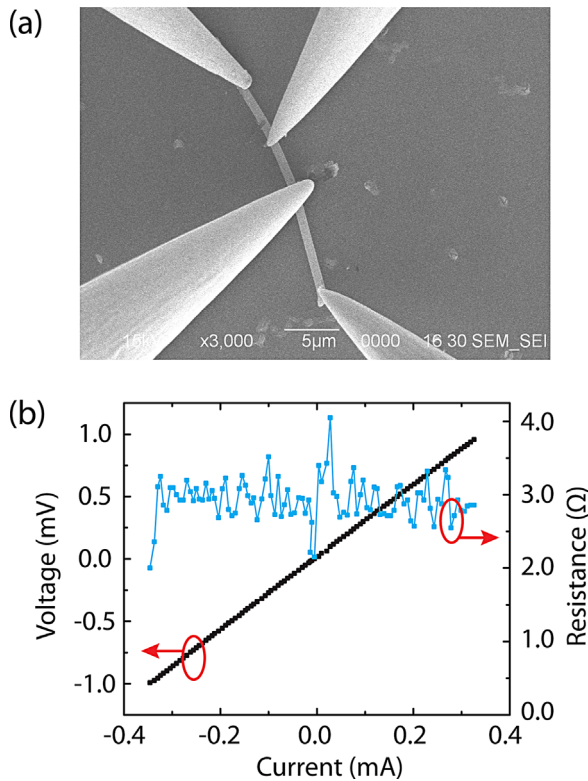


Figure 4 Four-probe resistivity measurement of as-grown Al NW. (a) Top view SEM of an Al NW on glass substrate contacted by four tungsten probes. (b) Four-probe $I-V$ measurement, with differential resistance dV/dI (blue) showing Ohmic behavior.

polarized white (halogen) light. The wires were transferred to a clean Si wafer by the pressing method. The polarization angle θ was defined in such a way that when $\theta = 0^\circ$ (90°), electric field is perpendicular (parallel) to the length of the wire. An SEM image of this measured Al NW was shown in Fig. 2(g). When tuning the polarization angle of the incident light, the color of the crescent-shaped Al NW changed from purple to orange, as shown in Fig. 6(a). 2D full-wave simulations were done on an Al NW with this same cross-section, as shown in Fig. 6(c). The simulation method is described in detail in reference [28]. The scattering spectrum was calculated by integrating the power flow density over a solid angle corresponding to the numerical aperture of 0.5 of the Olympus MPLN $50\times$ lens used for the observation, with an incidence angle of 60° (this is the angle between the incident vector k shown in Fig. 6(c) and the vertical axis). The scattering spectrum of the Al NW was further averaged over the two situations of light incident from the left- and right-hand-sides of the NW, to account for the asymmetric property of the crescent-shaped Al NW. The obtained scattering spectra under tuned polarization are shown in Fig. 6(b), and also converted into RGB colors using the CIE standard (detailed in Supporting Information), and shown in circles next to the Al NWs with corresponding polarization angles in Fig. 6(a). We see good agreement between the simulated and measured colors. The simulated electric field intensity profile of the crescent-shaped Al NW is shown in Fig. 6(d) for TM polarized ($\theta = 0^\circ$), 695 nm incidence. Enhanced localized electric fields are seen at the caw tips of the crescent, leading to large absorption (and

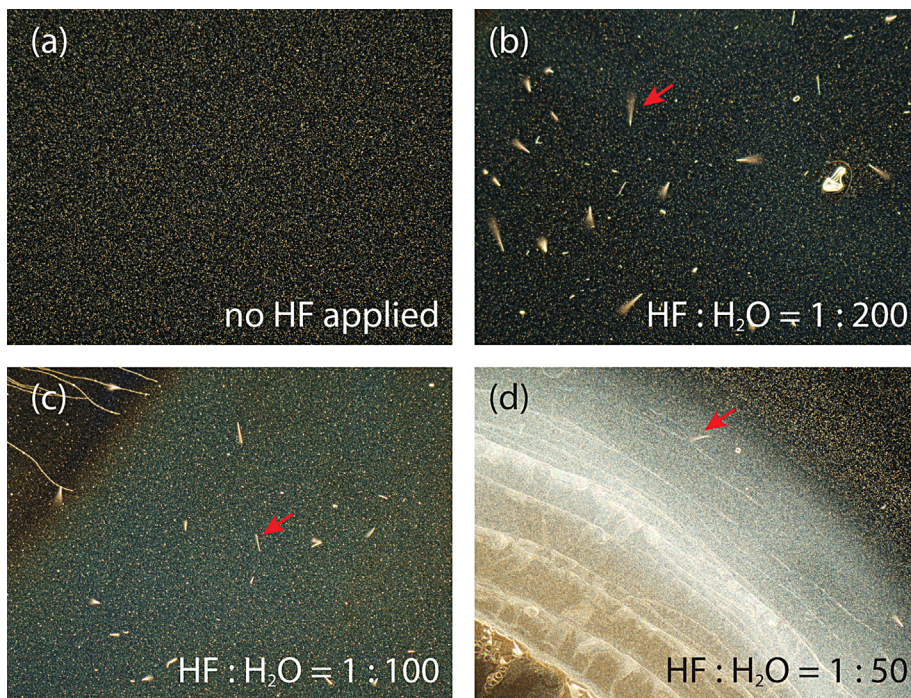


Figure 5 Dark field optical images of as-grown Al NWs under various HF concentrations. (a) No HF. HF:H₂O = (b) 1:200, (c) 1:100, and (d) 1:50. Red arrows indicate particular Al NWs.

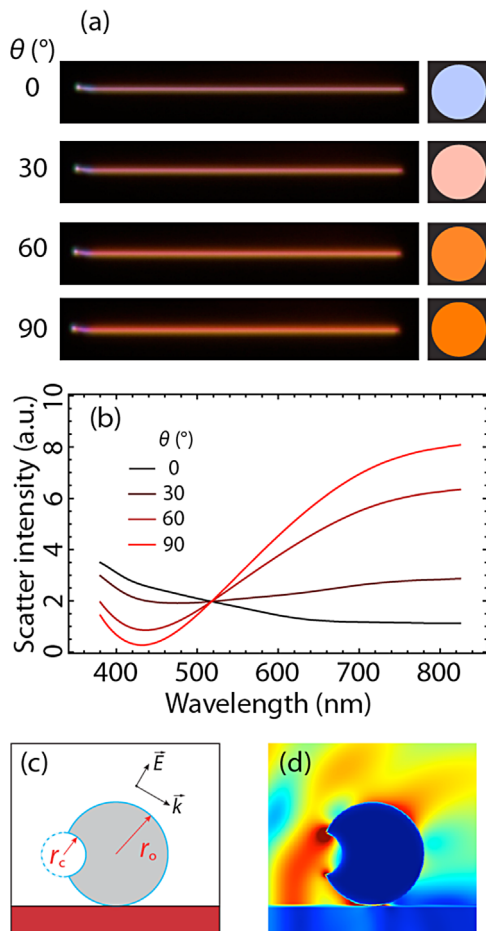


Figure 6 Optical analysis of a crescent-shaped Al NW. (a) Dark-field optical images of a 75 μm long crescent-shaped Al NW with tuned polarization. (b) Simulated dark-field scattering spectra of an Al NW with the same cross-section. Circles to the right of each Al NW image in (a) are RGB colors converted by the simulated spectra in (b) via the CIE standard. (c) Schematic cross-section of the crescent-shape Al NW shown in (a), with $r_c = 100\text{ nm}$ and $r_o = 235\text{ nm}$, covered by 5 nm native oxide (Al_2O_3) layer. Incident field is indicated by black arrows for $\theta = 0^\circ$ case. Red layer on the bottom indicates the Si substrate. (d) Simulated electric field intensity for crescent-shaped Al NW, under incident condition shown in (c).

thus small scattering) cross-section. The dielectric constants of Al [29], Al_2O_3 [30], and Si [31] were taken from their bulk values in the literature. The good match between the simulated spectra using bulk Al properties with the measured spectra further confirms the metallic property of these Al NWs.

We note that, at the present stage, we do not have an effective mechanism to control the shape of such Al NWs. Within all the cross-sections shown in this letter, the crescent, circle, and tube shapes are the most commonly observed. Other, more exotic shapes are also found, for example, double or multiple trenches along a cylinder. We infer that the shapes of the Al NWs are determined by the shapes of the impurities on the SiO_2 substrate (and/or access

ports on the Al_2O_3 surface). Also, the surface condition of the glass wafers is crucial for the formation of Al NWs. We see no Al NW growth on glass wafers cleaned by Ar plasma (2 min at 10 W and 0.4 Pa) in the sputtering system before depositing Al. This further implies that impurities on the glass substrates are crucial for the growth of the Al NWs. Finally, the working temperature is found to be within a 20 $^\circ\text{C}$ window around 250 $^\circ\text{C}$, outside of which leads to Al island formation.

4 Conclusions In conclusion, we have shown a convenient and rapid stress-induced growth process of Al NWs, controlled largely by the concentration of applied hydrofluoric acid. Multiple characterizations (including SEM, TEM, 4-probe resistivity, and dark-field optical images) have shown that the grown Al NWs are polycrystalline fcc Al structures with ultrasmooth surfaces (i.e., surface roughness less than 5 nm from SEM imaging), with many possible cross-section geometries, making them novel candidates for Al plasmonic investigations and applications. Although more work is needed to understand the NW preparation process, our results may be of interest in the fabrication and application of unconventional, nearly-one dimensional Al nanostructures.

Supporting Information

Additional supporting information may be found in the online version of this article at the publisher's website.

Acknowledgements The authors acknowledge partial support from W. M. Keck Foundation. F. Y. would like to thank Dr. Greg McMahon for assistance in the four-probe resistivity measurement of the Al NWs, and Dr. Dezhi Wang for assistance in the TEM image acquisition.

References

- [1] M. W. Knight, L. Liu, Y. Wang, L. Brown, S. Mukherjee, N. S. King, H. O. Everitt, P. Nordlander, and N. J. Halas, *Nano Lett.* **12**, 6000 (2012).
- [2] A. Moscatelli, *Nature Nanotechnol.* **7**, 778 (2012).
- [3] M. W. Knight, N. S. King, L. Liu, H. O. Everitt, P. Nordlander, and N. J. Halas, *ACS Nano* **8**, 834 (2014).
- [4] Y. T. Pang, G. W. Meng, L. D. Zhang, W. J. Shan, C. Zhang, X. Y. Gao, and A. W. Zhao, *Solid State Sci.* **5**, 1063 (2003).
- [5] D. D. Sung, M. S. Choo, J. S. Noh, W. B. Chin, and W. S. Yang, *Bull. Korean Chem. Soc.* **27**, 1159 (2006).
- [6] E. Perre, L. Nyholm, T. Gustafsson, P.-L. Taberna, P. Simon, and K. Edstrom, *Electrochem. Commun.* **10**, 1467 (2008).
- [7] K. K. Caswell, C. M. Bender, and C. J. Murphy, *Nano Lett.* **3**, 667 (2003).
- [8] T. Kijima, T. Yoshimura, M. Uota, T. Ikeda, D. Fujikawa, S. Mouri, and S. Uoyama, *Angew. Chem. Int. Ed.* **43**, 228 (2004).
- [9] C. J. Murphy, T. K. Sau, A. M. Gole, C. J. Orendorff, J. Gao, L. Gou, S. E. Hunyadi, and T. Li, *J. Phys. Chem. B* **109**, 13857 (2005).

- [10] I. A. Blech, P. M. Petroff, K. L. Tai, and V. Kumar, *J. Cryst. Growth* **32**, 161 (1975).
- [11] K. Hazama, Y. Nakamura, and O. Nittono, *Jpn. J. Appl. Phys.* **27**, 1142 (1988).
- [12] M. Chen, Y. Yue, and Y. Ju, *J. Appl. Phys.* **111**, 104305 (2012).
- [13] M. Saka and R. Nakanishi, *Mater. Lett.* **60**, 2129 (2006).
- [14] Y. Lu and M. Saka, *Mater. Lett.* **63**, 2294 (2009).
- [15] M. Suzuki, K. Nagai, S. Kinoshita, K. Nakajima, K. Kimura, T. Okano, and K. Sasakawa, *Appl. Phys. Lett.* **89**, 133103 (2006).
- [16] M. Suzuki, R. Kita, H. Hara, K. Hamachi, K. Nagai, K. Nakajima, and K. Kimura, *J. Electrochem. Soc.* **157**, K34 (2010).
- [17] A. Aubry, D. Y. Lei, A. I. Fernandez-Dominguez, Y. Sonnefraud, S. A. Maier, and J. B. Pendry, *Nano Lett.* **10**, 2574 (2010).
- [18] Y. Luo, D. Y. Lei, S. A. Maier, and J. B. Pendry, *Phys. Rev. Lett.* **108**, 023901 (2012).
- [19] D. K. Gramotnev, M. G. Nielsen, S. J. Tan, M. L. Kurth, and S. I. Bozhevolnyi, *Nano Lett.* **12**, 359 (2012).
- [20] A. M. Heikal, M. F. O. Hameed, and S. S. Obayya, *J. Lightwave Technol.* **31**, 2184 (2013).
- [21] J. Rybczynski, K. Kempa, A. Herczynski, Y. Wang, M. J. Naughton, Z. F. Ren, Z. P. Huang, D. Cai, and M. Giersig, *Appl. Phys. Lett.* **90**, 021104 (2007).
- [22] Y. Peng, X. Wang, and K. Kempa, *Opt. Express* **16**, 1758 (2008).
- [23] S. Aceto, C. Y. Chang, and R. W. Vook, *Thin Solid Films* **219**, 80 (1992).
- [24] C. Y. Chang and R. W. Vook, *Thin Solid Films* **228**, 205 (1993).
- [25] F. C. Nix and D. MacNair, *Phys. Rev.* **60**, 597 (1941).
- [26] J. B. Watchman, Jr., T. G. Scuderi, and G. W. Cleek, *J. Am. Ceram. Soc.* **45**, 319 (1962).
- [27] Standard reference material 731 NIST 1993, Gaithersburg, MD; http://glassproperties.com/references/NIST_Certificates/731_pg2.gif.
- [28] R. T. Hill, J. J. Mock, Y. Urzhumov, D. S. Sebban, S. J. Oldenburg, S.-Y. Chen, A. A. Lazarides, A. Chilkoti, and D. R. Smith, *Nano Lett.* **10**, 4150 (2010).
- [29] A. D. Rakic, A. B. Djuricic, J. M. Elazar, and M. L. Majewski, *Appl. Opt.* **37**, 5271 (1998).
- [30] I. H. Maliston, F. V. Murphy, Jr., and W. S. Rodney, *J. Opt. Soc. Am.* **48**, 72 (1958).
- [31] G. Vuye, S. Fisson, V. Nguyen Van, Y. Wang, J. Rivory, and F. Abeles, *Thin Solid Films* **233**, 166 (1993).